

ATTACHMENT 3

SEISMIC REFRACTION STUDY

For the Atlantic Coast Pipeline

George Washington National Forest and Monongahela National Forest
Virginia and West Virginia

PREPARED FOR:

Ms. Kathleen Harrison, PG
Geosyntec Consultants, Inc.
3990 Old Town Ave., Suite 101-A
Sand Diego, CA 92110

March 10th, 2017



Draper Aden Associates

Engineering • Surveying • Environmental Services

2206 South Main Street
Blacksburg, Virginia 24060
(540) 552-0444 • Fax (540) 552-0291
www.daa.com

March 10th, 2017

RE: Atlantic Coast Pipeline – Seismic Refraction Study, George Washington National Forest and Monongahela National Forest, Virginia and West Virginia
DAA Project Number: 16010129-010203

Ms. Kathleen Harrison, PG
Geosyntec Consultants, Inc.
3990 Old Town Ave., Suite 101-A
Sand Diego, CA 92110

Dear Ms. Harrison,

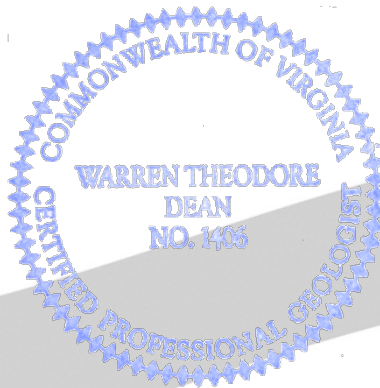
Draper Aden Associates has completed the seismic refraction study in the George Washington National Forest and the Monongahela National Forest for the Atlantic Coast Pipeline project. This study was undertaken to evaluate the depth to bedrock at a total of 124 soil test pit locations along the proposed pipeline route. The following report documents our methodologies and findings.

We value our professional relationship with Geosyntec, and hope that you will contact us with any similar needs in the future. If you have any questions regarding this report, or if we can be of any further service to you please do not hesitate to contact us.

Sincerely,



Warren T. "Ted" Dean, P.G.
Program Manager I



3RD PARTY REVIEW

This report has been subjected to technical and quality reviews by:

Christopher M. Printz, PG
Name:
Senior Project Geologist

Chris Printz
Signature



March 10th, 2017
Date

List of Figures

- Figure 1. Idealized cross-section of differential weathering.
- Figure 2. Map index for sheets 1 through 8.
- Figure 3. Map index for sheets 9 through 22.
- Figure 4. Map index for sheet 23.
- Figure 5. Map Sheet 1, seismic refraction line locations, test pits MNF-P003-161111 through MNF-P007-161111.
- Figure 6. Map Sheet 2, seismic refraction line locations, test pits MNF-P024-161110 through MNF-R026-161110.
- Figure 7. Map Sheet 3, seismic refraction line locations, test pits MNF-P033-161112 through MNF-P047-161112.
- Figure 8. Map Sheet 4, seismic refraction line locations, test pits MNF-P063-161111 through MNF-P073-161112.
- Figure 9. Map Sheet 5, seismic refraction line locations, test pits MNF-P077-161112 through MNF-P087-161111.
- Figure 10. Map Sheet 6, seismic refraction line locations, test pits GWNF-P098-161114 through GWNF-P111-161115.
- Figure 11. Map Sheet 7, seismic refraction line locations, test pits GWNF-P115-161115 through GWNF-P121-161111.
- Figure 12. Map Sheet 8, seismic refraction line locations, test pits GWNF-P132-161114 through GWNF-P135-161114.
- Figure 13. Map Sheet 9, seismic refraction line locations, test pits GWNF-P155-161115 through GWNF-P162-161115.
- Figure 14. Map Sheet 10, seismic refraction line locations, test pits GWNF-P165-161116 through GWNF-P172-161116.
- Figure 15. Map Sheet 11, seismic refraction line locations, test pits GWNF-P176-161116 through GWNF-P333-161116.
- Figure 16. Map Sheet 12, seismic refraction line locations, test pits GWNF-P352-161117 and GWNF-P352A-161117.
- Figure 17. Map Sheet 13, seismic refraction line locations, test pits GWNF-P195-161117 through GWNF-P199-161117.

- Figure 18. Map Sheet 14, seismic refraction line locations, test pits GWNF-P201-161117 through GWNF-P206-161117.
- Figure 19. Map Sheet 15, seismic refraction line locations, test pits GWNF-P211-161117 and GWNF-P213-161117.
- Figure 20. Map Sheet 16, seismic refraction line locations, test pits GWNF-P221-161201 through GWNF-P223-161201.
- Figure 21. Map Sheet 17, seismic refraction line locations, test pits GWNF-P225-161118 through GWNF-P239A-161118.
- Figure 22. Map Sheet 18, seismic refraction line locations, test pits GWNF-P242-161118 through GWNF-P253-161118.
- Figure 23. Map Sheet 19, seismic refraction line locations, test pits GWNF-P261-161118 through GWNF-P277-161201.
- Figure 24. Map Sheet 20, seismic refraction line locations, test pits GWNF-P278-161201 through GWNF-P286-161201.
- Figure 25. Map Sheet 21, seismic refraction line locations, test pits GWNF-P290-161201 through GWNF-P304-161201.
- Figure 26. Map Sheet 22, seismic refraction line locations, test pits GWNF-P308-161201 through GWNF-P314-161201.
- Figure 27. Map Sheet 23, seismic refraction line locations, test pits GWNF-P315-161202 through GWNF-R007-161202.
- Figure 28. Seismic refraction model results for MNF-P003-161111 and MNF-P004-161111.
- Figure 29. Seismic refraction model results for MNF-P005-161111 and MNF-P006-161111.
- Figure 30. Seismic refraction model results for MNF-P007-161111 and MNF-P010-161111.
- Figure 31. Seismic refraction model results for MNF-P24-161108 and MNF-R28-161110.
- Figure 32. Seismic refraction model results for MNF-R29-161110 and MNF-R26-161110.
- Figure 33. Seismic refraction model results for MNF-P033-161112 and MNF-P040-161112.
- Figure 34. Seismic refraction model results for MNF-P045-161112 and SSF-P047-161112.
- Figure 35. Seismic refraction model results for MNF-P063-161111 and MNF-R019-161112.
- Figure 36. Seismic refraction model results for MNF-P066-161111 and MNF-R067-161112.
- Figure 37. Seismic refraction model results for MNF-R073-161112 and MNF-R077-161112.

- Figure 38. Seismic refraction model results for MNF-R078-161112 and MNF-P087-161111.
- Figure 39. Seismic refraction model results for GWNF-P098-161114 and GWNF-P099-161114.
- Figure 40. Seismic refraction model results for GWNF-P109-161115 and GWNF-P110-161115.
- Figure 41. Seismic refraction model results for GWNF-P111-161115 and GWNF-P115-161115.
- Figure 42. Seismic refraction model results for GWNF-P119-161115 and GWNF-P120-161111.
- Figure 43. Seismic refraction model results for GWNF-P120A-161111 and GWNF-P121-161111.
- Figure 44. Seismic refraction model results for GWNF-P132-161114 and GWNF-P134-161114.
- Figure 45. Seismic refraction model results for GWNF-P135-161114 and GWNF-P155-161115.
- Figure 46. Seismic refraction model results for GWNF-P156-161115 and GWNF-P157-161115.
- Figure 47. Seismic refraction model results for GWNF-P158-161115 and GWNF-P159-161115.
- Figure 48. Seismic refraction model results for GWNF-P160-161115 and GWNF-P162-161115.
- Figure 49. Seismic refraction model results for GWNF-P165-161115 and GWNF-P166-161115.
- Figure 50. Seismic refraction model results for GWNF-P167-161116 and GWNF-P172-161116.
- Figure 51. Seismic refraction model results for GWNF-P176-161116 and GWNF-P177-161116.
- Figure 52. Seismic refraction model results for GWNF-P179-161116 and GWNF-P180-161116.
- Figure 53. Seismic refraction model results for GWNF-P181-161116 and GWNF-P182-161116.
- Figure 54. Seismic refraction model results for GWNF-P183-161116 and GWNF-P333-161116.

- Figure 55. Seismic refraction model results for GWNF-P352-161117, GWNF-P352A-161117, and GWNF-P195-161117.
- Figure 56. Seismic refraction model results for GWNF-P196-161117 and GWNF-P197-161117.
- Figure 57. Seismic refraction model results for GWNF-P199-161117 and GWNF-P201-161117.
- Figure 58. Seismic refraction model results for GWNF-P203-161117 and GWNF-P204-161117.
- Figure 59. Seismic refraction model results for GWNF-P205-161117 and GWNF-P206-161117.
- Figure 60. Seismic refraction model results for GWNF-P211-161117 and GWNF-P213-161117.
- Figure 61. Seismic refraction model results for GWNF-P221-161201 and GWNF-P222-161201.
- Figure 62. Seismic refraction model results for GWNF-R010-161201 and GWNF-R011-161201.
- Figure 63. Seismic refraction model results for GWNF-P223-161201 and GWNF-P225A-161118.
- Figure 64. Seismic refraction model results for GWNF-P225-161118 and GWNF-P225B-161118.
- Figure 65. Seismic refraction model results for GWNF-P228-161118 and GWNF-P229-161118.
- Figure 66. Seismic refraction model results for GWNF-R018-161118 and GWNF-R015-161118.
- Figure 67. Seismic refraction model results for GWNF-P237-161118 and GWNF-P239-161118.
- Figure 68. Seismic refraction model results for GWNF-P239A-161118 and GWNF-P242-161118.
- Figure 69. Seismic refraction model results for GWNF-P252-161118 and GWNF-P253-161118.
- Figure 70. Seismic refraction model results for GWNF-P261-161118 and GWNF-P264-161118.
- Figure 71. Seismic refraction model results for GWNF-P276-161201 and GWNF-P277-161201.

- Figure 72. Seismic refraction model results for GWNF-P278-161201 and GWNF-P279B-161201.
- Figure 73. Seismic refraction model results for GWNF-P279-161201, GWNF-P279A-161201, and GWNF-P283-161201.
- Figure 74. Seismic refraction model results for GWNF-P286-161201 and GWNF-P290-161201.
- Figure 75. Seismic refraction model results for GWNF-P299-161201 and GWNF-P303-161201.
- Figure 76. Seismic refraction model results for GWNF-P304-161201 and GWNF-P308-161201.
- Figure 77. Seismic refraction model results for GWNF-P310-161201 and GWNF-R014-161201.
- Figure 78. Seismic refraction model results for GWNF-R012-161201 and GWNF-P314-161201.
- Figure 79. Seismic refraction model results for GWNF-R007-161202 and GWNF-P331-161202.
- Figure 80. Seismic refraction model results for GWNF-P328-161202 and GWNF-P327-161202.
- Figure 81. Seismic refraction model results for GWNF-P326-161202 and GWNF-P325-161202.
- Figure 82. Seismic refraction model results for GWNF-P324-161202 and GWNF-P323-161202.
- Figure 83. Seismic refraction model results for GWNF-R003-161202, GWNF-R001-161202, and GWNF-R002-161202.
- Figure 84. Seismic refraction model results for GWNF-P322-161202 and GWNF-P321-161202.
- Figure 85. Seismic refraction model results for GWNF-R006-161202 and GWNF-P319-161202.
- Figure 86. Seismic refraction model results for GWNF-P318-161202 and GWNF-R005-161202.
- Figure 87. Seismic refraction model results for GWNF-R004-161202 and GWNF-P316-161202.
- Figure 88. Seismic refraction model results for GWNF-P315-161202.

List of Tables

Table 1. Depth to Rock and Weathered Rock from the Seismic Refraction Data.....	8
---	---

Table of Contents

- EXECUTIVE SUMMARY1**
- 1.0 INTRODUCTION3**
- 2.0 SITE GEOLOGY.....3**
- 3.0 SEISMIC REFRACTION4**
 - 3.1 Principles of Seismic Refraction..... 4
 - 3.2 Field Methods 5
 - 3.3 Seismic Data Processing 6
- 4.0 SEISMIC REFRACTION RESULTS6**
- 5.0 LIMITATIONS12**
- 6.0 REFERENCES13**
- 7.0 FIGURES.....14**

EXECUTIVE SUMMARY

Draper Aden Associates was retained by Geosyntec Consultants, Inc. (Geosyntec) to conduct a seismic refraction study for the proposed Atlantic Coast Pipeline (ACP) throughout portions of the ACP corridor that crosses through the George Washington National Forest (GWNF) and Monongahela National Forest (MNF) in Virginia and West Virginia. Specifically, this study was initiated to identify the bedrock depth in soil test pits excavated during completion of an Order 1 Soil Survey that did not encounter bedrock within their protocol depths. The soil test pits were hand-dug approximately every 350 feet through the GWNF and MNF along the proposed pipeline route bedrock or to a depth of 50 inches, whichever was encountered first, and 124 of those pits did not encounter bedrock within the excavated depth. Data for seismic refraction profiles were collected for each of the 124 soil test pit locations with the purpose of determining the depth to bedrock. The seismic refraction survey was completed between November and December 2016.

The study area is spread across a broad geographic area, and as such, it is underlain by a variety of lithologies. The majority of the study area is located within the Valley and Ridge geologic and physiographic province, which consists of elongate parallel mountain ridges and valleys that are underlain by folded and faulted Paleozoic sedimentary bedrock. These parallel ridges and valleys are the result of differential weathering of layered clastic and carbonate bedrock. The majority of the study area is underlain by sedimentary bedrock formations of varying ages consisting of limestone, sandstone, shale, siltstone, mudstone, and coal.

The test pit locations were grouped into 23 map sheets that cover a distance of about 82 miles, from mile markers 73 to 155. The locations of the test pits and geophones for each seismic line are provided in large format maps, and the cross-sections for each seismic line depict the pit locations on each profile as well as the depth to rock at each pit location.

The literature suggest a wide range of potential P-wave velocity values for weathered and unweathered sedimentary rocks, suggesting that velocities for weathered, fractured, or decomposed rock range from 610 meters per second (2,000 feet per second) to 3,049 meters per second (10,000 feet per second), and that P-wave velocities of saturated shale and sandstone range from 1,100 meters per second (3,600 feet per second) to 5,100 meters per second (17,000 feet per second), with velocities of limestone up to 6,000 meters per second (20,000 feet per second). It

should be noted that saturated conditions tend to facilitate P-wave propagation, and thus the velocities of dry rocks will be somewhat lower than those described in these references.

The cross-sections for each seismic line are presented as tomographic velocity-depth models which give modeled P-wave velocities in feet per second, color contoured as a function of depth. Based on our previous experience, the top of weathered rock is interpreted as the P-wave velocity at which the velocity contours begin to compress and become closer together. The top of unweathered rock is interpreted to be the P-wave velocity at which the velocity contours become even more tightly compressed. For weathered bedrock, this usually occurs at velocities between 2,000 feet per second and 3,500 feet per second, and for unweathered rock between 3,500 feet per second and 7,000 feet per second. The interpreted weathered rock surface is indicated in each of the sections by a dashed black line, and the top of unweathered rock is indicated in each of the sections by a solid black line. For those cases where the interpretation of these surfaces is ambiguous or where more than one interpretation for either surface is possible, a conservative approach was applied where 2,000 feet per second was used as the weathered rock surface and 3,500 feet per second as the unweathered rock surface. The study area crosses numerous geologic settings and lithologies, so there is a wide range in velocities represented in the seismic sections

1.0 INTRODUCTION

Draper Aden Associates was retained by Geosyntec Consultants, Inc. (Geosyntec) to conduct a seismic refraction study for the proposed Atlantic Coast Pipeline (ACP) throughout portions of the ACP corridor that crosses through the George Washington National Forest (GWNF) and Monongahela National Forest (MNF) in Virginia and West Virginia. Specifically, this study was initiated to identify the bedrock depth in soil test pits excavated during completion of an Order 1 Soil Survey that did not encounter bedrock within their protocol depths. The soil test pits were hand-dug approximately every 350 feet through the GWNF and MNF along the proposed pipeline route to bedrock, or to a depth of 50 inches, whichever was encountered first, and 124 of those pits did not encounter bedrock within the excavated depth. Data for seismic refraction profiles were collected for between November 10 and 18, 2016 and on December 1 and 2, 2016 for each of these 124 soil test pit locations with the purpose of determining the depth to bedrock.

2.0 SITE GEOLOGY

The study area is spread across a broad geographic area, and as such, it is underlain by a variety of lithologies. The majority of the study area is located within the Valley and Ridge geologic and physiographic province, which consists of elongate parallel mountain ridges and valleys that are underlain by folded and faulted Paleozoic sedimentary bedrock. These parallel ridges and valleys are the result of differential weathering of layered clastic and carbonate bedrock on a regional scale. The ridges tend to be comprised of sandstone and conglomerates, which are resistant to physical weathering and the valleys tend to be comprised of carbonates and fine grained clastic materials that are more susceptible to physical weathering.

In folded and faulted terrains of varying lithologies, there exists the potential for strongly variable weathering profiles on a local or sub-regional scale, especially with carbonate rocks. Joints, fractures, and bedding planes provide greater surface area for physical weathering, so more highly fractured rock will tend to weather into soil more readily than unfractured rock. These structural features are avenues for water infiltration and therefore can increase the rate of chemical dissolution and weathering of carbonate rocks. Therefore, localized differential weathering can

result in a highly variable overburden thickness. An idealized cross-section of variable soil thickness from differential weathering is provided in Figure 1 (From Fookes, 1997).

3.0 SEISMIC REFRACTION

3.1 Principles of Seismic Refraction

Seismic compressional waves (P-waves) are emitted through use of an energy source, such as a sledgehammer on a steel plate, which produces pulses of seismic energy. The ground motion from the seismic energy is recorded by an array of geophones spaced at regular intervals along a desired survey line. As the survey progresses, the source location moves along the extent of the survey line and beyond to obtain travel times from seismic waves to geophones at the surface. These travel times are recorded in the field by a seismograph, and analyzed using seismic refraction processing software during data analysis.

For analysis of seismic refraction data there are a set of assumptions. The first assumption is that the subsurface is composed of a stack of geologic layers separated by planar surfaces. This assumption is usually valid since the principle application of seismic refraction is to look for the bedrock surface or the boundaries between sedimentary layers. The second assumption is that seismic velocities increase with depth. This assumption is valid when exploring for the bedrock surface, or in unconsolidated sediments when fine-grained materials are underlain by coarse-grained materials. The third assumption is that the velocity within each layer is uniform (Griffiths and King, 1988).

The primary data of interest in seismic refraction studies are the travel times of the seismic waves as they first arrive at the geophones, called first arrivals or first breaks. As the waves travel through the subsurface they propagate in all directions. For those geophones closest to the source, the first arrivals are often from direct waves as they travel along the ground surface. However, those waves traveling downward eventually reach a higher-velocity surface along which they travel faster than those waves traveling through the upper layer, and waves refracted from the higher-velocity layer begin to arrive at the geophones before the direct waves. In the travel time graphs, the point at which the refracted waves begin to arrive before the direct waves is characterized by a change in slope of the arrival times.

3.2 Field Methods

The seismic refraction survey was conducted using a series of twenty-four 4.5-Hz geophones, spaced 5 feet apart for a total seismic line spread of 115 feet for each of the 124 test pits. Three seismic lines were able to span two test pits each, making a total of 121 seismic lines for the 124 test pits.

Each line spread was oriented to minimize topographic variation, as several locations occurred along steep slopes or difficult terrain. Orienting the line spreads in this manner allowed for safer working conditions, and ease of access along the survey area. This approach was also conducive towards the processing and modeling of seismic refraction data as the terrain over which seismic data were collected factored into the modeling process. Steep terrain tends to make it more difficult for the seismic modeling to converge to a satisfactory solution.

The geophones were connected via a seismic cable to a Geometrics Geode seismograph. Refraction data were collected from five shot point (energy source) locations located along each spread. The source consisted of a sledgehammer striking a metal plate at each of the shot point locations. Seismic refraction data were “stacked” to a minimum of five hammer strikes per shot point location. The shot point locations were distributed within and beyond the extents of the geophone spread, with a central shot point in the middle of the spread. In instances where a test pit location could not be definitively identified due to ground disturbance, the seismic refraction line was centered on the GPS coordinate of the pit, or on surface features indicative of previous disturbance in the vicinity of the test pit coordinates. Some of the pits were spaced close enough together to allow two pits to be covered with a single seismic refraction line. The seismic survey identification numbers (e.g. MNF-P003-161111) were named using the following convention: forest location (i.e. MNF or GWNF), followed by the first four alphabetic and numeric characters of the soil survey pit I.D. number, (e.g. P-003), and the seismic survey date (year, month, day). Table 1 cross references the seismic survey pit I.D. and the soil survey pit I.D.

The locations of the pits were recorded with a Trimble 6H Pro GPS receiver capable of sub-meter accuracy. In addition, the location of the first and last geophones were recorded as well as several intermediate geophone locations, usually every fifth geophone. The locations of the geophones that were not recorded with GPS were interpolated from the recorded points.

3.3 Seismic Data Processing

The refraction data were processed using the SeisImager software program. The SeisImager program allows the user to identify the first arrivals for each shot point, with subsequent interpretation of the corresponding slope breaks in the arrival time graph. These data serve as the input to tomographic modeling. Seismic refraction tomography is an iterative modeling process by which the observed travel times are compared to an initial earth model or tomograph. The tomographic process then calculates the travel times that would occur if the earth model were correct. The earth model is then adjusted to minimize the difference between the observed travel times and the modeled travel times. When a close match is obtained between the calculated travel times and the observed travel times, the earth model can be accepted as a reasonable representation of actual conditions. For this study, the acceptable tolerance between the calculated and observed travel times was defined as a root mean squared (RMS) error of 2 milliseconds or less. All of the seismic sections for this study met or exceeded this criterion.

The geophone locations were plotted onto LIDAR topography data provided by Geosyntec. The elevations of each geophone were extracted from the LIDAR data and were incorporated into the seismic data processing, so that the model would consider the topography in the inversion modeling process and the resulting profiles would reflect the local relief.

4.0 SEISMIC REFRACTION RESULTS

The test pit locations were grouped into 23 map sheets that cover a distance of about 82 miles, from mile markers 73 to 155 (Figures 2 through 4). Map Sheets 1 through 23 (Figures 5 through 27) illustrate the geophone spreads and orientations plotted on shaded relief maps constructed from the LIDAR data.

The literature suggest a wide range of potential P-wave velocity values for weathered and unweathered sedimentary rocks. Reddy (2011) cites velocities for weathered, fractured, or decomposed rock as ranging from 610 meters per second (2,000 feet per second) to 3,049 meters per second (10,000 feet per second). Bourbié et. al. (1987) describe the P-wave velocity of saturated shale to range from 1,100 meters per second (3,600 feet per second) to 2,500 meters per second (8,200 feet per second) and saturated sandstone to range from 2,000 meters per second

(6,500 feet per second) to 3,500 meters per second (11,500 feet per second). Griffiths and King (1988) give the velocities of saturated shale and sandstone to range from approximately 1,200 meters per second (3,900 feet per second) to 5,100 meters per second (17,000 feet per second), and velocities of limestone up to 6,000 meters per second (20,000 feet per second). It should be noted that saturated conditions tend to facilitate P-wave propagation, and thus the velocities of dry rocks will be somewhat lower than those described in these references.

The cross-sections for each seismic line are presented in Figures 28 through 88 in order from west to east. The seismic sections are provided as tomographic velocity-versus-depth models which give modeled P-wave velocities in feet per second, color-contoured as a function of depth. Based on our previous experience, the top of weathered rock is generally interpreted as the P-wave velocity at which the velocity contours begin to compress and become closer together, usually at velocities between 2,000 feet per second and 3,500 feet per second. The top of unweathered rock is generally interpreted to be the P-wave velocity at which the velocity contours become even more tightly compressed, which usually occurs at velocities between 3,500 feet per second and 7,000 feet per second. The interpreted weathered rock surface is indicated in each of the sections by a dashed black line, and the interpreted top of unweathered rock is indicated in each of the sections by a solid black line. For those cases where the interpretation of these surfaces is ambiguous or where more than one interpretation for either surface is possible, a conservative approach was applied where 2,000 feet per second was used as the weathered rock surface and 3,500 feet per second as the rock surface. Specifically, the tomographs from MNF-P024-161108 and GWNF-P157-161115 display very low velocities with little of the characteristic compressing of the velocity contours that would clearly indicate transitional surfaces. The tomographs for GWNF-P182-161116 and GWNF-P183-161116 display no velocities greater than 3,500 feet per second which is the lowest threshold described in the literature to describe unweathered rock. Therefore, it is likely that the rock is fractured or weathered through the depth of the model.

As discussed in Section 2.0, the study area crosses numerous lithologies, so there is a wide range in modeled bedrock velocities represented in the seismic sections, from 3,000 feet per second in GWNF-P182-161116 to 20,000 feet per second in GWNF-P277-161201. All of the interpreted depth-to-weathered-rock and depth-to-rock data are summarized in Table 1.

Table 1. Depth to Rock and Weathered Rock from the Seismic Refraction Data.

Pit ID	Soil Survey Pit ID	Lat	Long	Depth to Weathered Rock (ft)	Depth to Rock (ft)
MNF-P003-161111	P-003-160620-1025-rll	38.35490086° N	80.04292595° W	5.6	15.7
MNF-P004-161111	P-004-160620-1035-rll	38.35432460° N	80.04172007° W	10.7	13.6
MNF-P005-161111	P-005-160620-1425-rll	38.35357527° N	80.04100721° W	12.1	14.9
MNF-P006-161111	P-006-160620-1509-dat	38.35289138° N	80.04049981° W	7.8	8.9
MNF-P007-161111	P-007-160620-1245-dat	38.35206230° N	80.03963907° W	7.0	9.1
MNF-P010-161111	P-010-160620-1315-mgw	38.34960195° N	80.03756619° W	5.8	7.9
MNF-P024-161110	P-024-160614-1440-jsw	38.30775902° N	79.88143953° W	6.2	24.7
MNF-R028-161110	R-028-160513-1210-mpc	38.30716562° N	79.88097337° W	13.3	16.6
MNF-R029-161110	R-029-160513-1300-mpc	38.30627551° N	79.87955032° W	12.8	18.2
MNF-R026-161110	R-026-160513-1000-mpc	38.30382443° N	79.87654504° W	13.2	17.1
MNF-P033-161112	P-033-160615-1041-jsw	38.29981169° N	79.86502923° W	4.9	6.5
MNF-P040-161112	P-040-160615-1119-jcr	38.30251032° N	79.85807491° W	0.0	7.3
MNF-P045-161112	P-045-160614-1019-jcr	38.30190340° N	79.85254989° W	5.7	6.9
MNF-P047-161112	P-047-160614-1045-def	38.30174906° N	79.84949341° W	5.7	7.9
MNF-P063-161111	P-063-160614-0950-rll	38.29562426° N	79.83407130° W	5.9	7.6
MNF-R019-161112	R-019-160512-1020-mpc	38.29620147° N	79.83050436° W	6.2	10.5
MNF-P066-161111	P-066-160614-1040-rll	38.29641564° N	79.82956511° W	5.6	7.7
MNF-P067-161112	P-067-160614-1441-sdd	38.29720500° N	79.82898938° W	6.7	10.7
MNF-P073-161112	P-073-160616-1402-sdd	38.30062776° N	79.82392457° W	8.0	10.1
MNF-P077-161112	P-077-160617-1035-sdd	38.30381810° N	79.82143421° W	7.2	11.8
MNF-P078-161112	P-078-160617-1201-sdd	38.30464738° N	79.82105408° W	18.3	20.6
MNF-P087-161111	P-087-160616-1316-jcr	38.30392682° N	79.81277271° W	8.7	11.4
GWNF-P098-161114	P-098-160609-1040-def	38.30325388° N	79.80072335° W	6.7	8.4
GWNF-P099-161114	P-099-160609-1055-def	38.30254125° N	79.79933409° W	6.2	11.4
GWNF-P109-161115	P-109-160613-1321-sdd	38.30129483° N	79.78855656° W	10.8	19.0
GWNF-P110-161115	P-110-160613-1503-sdd	38.30113987° N	79.78720597° W	17.0	29.9
GWNF-P111-161115	P-111-160613-1602-sdd	38.30170861° N	79.78655746° W	18.2	25.8
GWNF-P115-161115	P-115-160613-1227-jcr	38.30363550° N	79.78186003° W	5.0	6.4
GWNF-P119-161115	P-119-160616-1020-mgw	38.30496109° N	79.77750190° W	9.3	11.4

Pit ID	Soil Survey Pit ID	Lat	Long	Depth to Weathered Rock (ft)	Depth to Rock (ft)
GWNF-P120-161111	P-120-160616-1010-mgw	38.30525469° N	79.77625552° W	6.5	12.5
GWNF-P120A-161111	P-120A-160616-1225-mgw	38.30536791° N	79.77599210° W	7.3	9.5
GWNF-P121-161111	P-121-160616-0950-mgw	38.30550261° N	79.77541247° W	6.6	8.8
GWNF-P132-161114	P-132-160615-1110-rll	38.30534354° N	79.76343708° W	9.1	12.5
GWNF-P134-161114	P-134-160615-1506-sdd	38.30368414° N	79.76235113° W	16.4	24.9
GWNF-P135-161114	P-135-160615-1321-sdd	38.30285397° N	79.76240084° W	6.1	8.3
GWNF-P155-161115	P-155-160606-1110-dat	38.18116501° N	79.67660280° W	8.9	11.5
GWNF-P156-161115	P-156-160606-1355-dat	38.18050631° N	79.67580883° W	7.3	10.2
GWNF-P157-161115	P-157-160606-1512-dat	38.17964400° N	79.67497274° W	11.6	24.7
GWNF-P158-161115	P-158-160606-1717-jsw	38.17895624° N	79.67419407° W	3.1	7.5
GWNF-P159-161115	P-159-160606-1400-jsw	38.17838394° N	79.67331980° W	8.7	21.7
GWNF-P160-161115	P-160-160606-1210-jsw	38.17786359° N	79.67218169° W	7.9	10.0
GWNF-P162-161115	P-162-160606-1040-jsw	38.17715978° N	79.67041712° W	8.8	10.0
GWNF-P165-161116	P-163-160620-1126-jsw	38.15410319° N	79.63169299° W	8.4	14.9
GWNF-P166-161116	P-164-160620-1117-jsw	38.15357147° N	79.63101624° W	7.3	9.9
GWNF-P167-161116	P-165-160620-1112-jsw	38.15288227° N	79.63061939° W	8.9	13.3
GWNF-P172-161116	P-172-160620-1117-def	38.14855009° N	79.62847048° W	6.8	9.2
GWNF-P176-161116	P-176-160621-1155-rll	38.13801967° N	79.63107017° W	7.6	29.8
GWNF-P177-161116	P-177-160622-1027-jsw	38.13725083° N	79.63101444° W	8.8	38.5
GWNF-P179-161116	P-179-160621-1215-jsw	38.13597696° N	79.62955630° W	9.5	27.6
GWNF-P180-161116	P-180-160621-1252-jsw	38.13531238° N	79.62866969° W	9.9	21.7
GWNF-P181-161116	P-181-160621-1300-jsw	38.13474262° N	79.62742029° W	10.4	35.0
GWNF-P182-161116	P-182-160621-1310-jsw	38.13433457° N	79.62635120° W	19.7	46.9
GWNF-P183-161116	P-183-160621-1318-jsw	38.13427412° N	79.62517148° W	15.9	59.4
GWNF-P333-161116	P-333-160621-1327-jsw	38.13412024° N	79.62420961° W	11.3	16.4
GWNF-P352A-161217	P-352A-160621-1147-mgw	38.11862266° N	79.59748665° W	4.2	7.6
GWNF-P352-161217	P-352-160621-1145-def	38.11861202° N	79.59724273° W	6.2	10.7
GWNF-P195-161217	P-195-160608-1325-sdd	38.14165918° N	79.47802563° W	7.2	9.5
GWNF-P196-161217	P-196-160608-1157-sdd	38.14199601° N	79.47745443° W	10.8	23.6
GWNF-P197-161217	P-197-160608-1047-sdd	38.14316797° N	79.47597138° W	10.8	20.4

Pit ID	Soil Survey Pit ID	Lat	Long	Depth to Weathered Rock (ft)	Depth to Rock (ft)
GWNF-P199-161217	P-199-160608-0856-sdd	38.14373011° N	79.47521422° W	7.4	9.2
GWNF-P201-161117	P-201-160603-1326-jsw	38.15226934° N	79.46983565° W	7.3	8.4
GWNF-P203-161117	P-203-160603-1129-sdd	38.15409079° N	79.46857130° W	7.1	13.8
GWNF-P204-161117	P-204-160603-0939-sdd	38.15456891° N	79.46784160° W	13.6	23.3
GWNF-P205-161117	P-205-160603-1155-jsw	38.15539773° N	79.46720331° W	10.2	26.7
GWNF-P206-161117	P-206-160603-0930-jsw	38.15604536° N	79.46599835° W	7.6	10.0
GWNF-P211-161117	P-211-160602-1149-sdd	38.15937572° N	79.46181169° W	7.8	8.8
GWNF-P213-161117	P-213-160602-1236-jsw	38.16094810° N	79.46020505° W	11.3	15.5
GWNF-P221-161201	P-221-160607-1223-dat	38.28032496° N	79.30771539° W	12.5	14.7
GWNF-P222-161201	P-222-160607-1055-dat	38.27985025° N	79.30640795° W	7.8	9.5
GWNF-R010-161201	R-010-160510-0925-mpc	38.27998498° N	79.30533025° W	8.9	11.8
GWNF-R011-161201	R-011-160510-0935-mpc	38.27937852° N	79.30491858° W	6.8	8.8
GWNF-P223-161201	P-223-160607-0910-dat	38.27959242° N	79.30446720° W	8.8	10.3
GWNF-P225-161118	P-225-160601-1130-mel	38.28125832° N	79.29318620° W	6.0	8.6
GWNF-P225A-161118	P-225A-160601-1130-jcr	38.28104850° N	79.29282389° W	5.8	7.8
GWNF-P225B-161118	P-225B-160601-1312-sdd	38.28160266° N	79.29266271° W	12.9	14.9
GWNF-P228-161118	P-228-160610-0907-def	38.28370715° N	79.29071897° W	5.1	7.5
GWNF-P229-161118	P-229-160610-0900-def	38.28371310° N	79.28963634° W	7.0	8.8
GWNF-R018-161118	R-018-160511-1145-mpc	38.28393792° N	79.28869706° W	5.5	7.0
GWNF-R015-161118	R-015-160511-0900-mpc	38.28398225° N	79.28674782° W	5.1	7.9
GWNF-P237-161118	P-237-160607-1240-mel	38.28608748° N	79.28103924° W	7.5	9.3
GWNF-P239-161118	P-239-160607-1427-def	38.28761625° N	79.27877382° W	6.0	7.9
GWNF-P239A-161118	P-239A-160607-1430-def	38.28736465° N	79.27863475° W	7.3	9.4
GWNF-P242-161118	P-242-160607-0920-def	38.28927081° N	79.27599253° W	5.7	7.7
GWNF-P252-161118	P-252-160608-1452-mel	38.29065799° N	79.26494383° W	6.9	8.8
GWNF-P253-161118	P-253-160608-0950-mel	38.29074112° N	79.26346393° W	5.2	15.5
GWNF-P261-161118	P-261-160609-0920-jsw	38.28816155° N	79.25584305° W	8.4	14.1
GWNF-P264-161118	P-264-160609-1425-jsw	38.28923828° N	79.25263375° W	11.0	14.0
GWNF-P276-161201	P-276-160610-0838-jsw	38.29149167° N	79.23875864° W	5.2	7.4
GWNF-P277-161201	P-277-160610-0841-sdd	38.29163204° N	79.23799290° W	6.8	10.2

Pit ID	Soil Survey Pit ID	Lat	Long	Depth to Weathered Rock (ft)	Depth to Rock (ft)
GWNF-P278-161201	P-278-160610-1143-sdd	38.29163347° N	79.23648555° W	5.9	7.5
GWNF-P279B-161201	P-279B-160610-1249-sdd	38.29189482° N	79.23564589° W	7.3	9.0
GWNF-P279-161201	P-279-160610-1359-dat	38.29214025° N	79.23442164° W	5.6	10.9
GWNF-P279A-161201	P-279A-160610-1450-def	38.29218017° N	79.23466691° W	5.4	11.2
GWNF-P283-161201	P-283-160606-0743-def	38.28943187° N	79.22228605° W	8.7	11.8
GWNF-P286-161201	P-286-160606-0808-def	38.28860992° N	79.21937811° W	10.6	13.6
GWNF-P290-161201	P-290-160606-1445-mel	38.28915547° N	79.21466057° W	8.7	14.1
GWNF-P299-161201	P-299-160603-0820-def	38.29112147° N	79.20415433° W	9.6	10.6
GWNF-P303-161201	P-303-160603-0830-mgw	38.29187981° N	79.19968308° W	7.5	9.2
GWNF-P304-161201	P-304-160603-0815-mgw	38.29169994° N	79.19825517° W	9.1	11.9
GWNF-P308-161201	P-308-160602-1231-jcr	38.29144717° N	79.19458127° W	9.2	10.7
GWNF-P310-161201	P-310-160603-0835-jcr	38.29027157° N	79.19125375° W	12.6	16.0
GWNF-R014-161201	R-014-160510-1530-mpc	38.28942480° N	79.19054918° W	10.8	13.8
GWNF-R012-161201	R-012-160510-1445-mpc	38.28913944° N	79.18966575° W	8.3	13.2
GWNF-P314-161201	P-314-160602-1115-mel	38.28856723° N	79.18793331° W	8.1	11.9
GWNF-R007-161202	R-007-160509-1550-mpc	37.94559534° N	78.95974387° W	7.9	12.0
GWNF-P331-161202	P-331-161011-0845-def	37.94545882° N	78.95946337° W	4.7	7.8
GWNF-P328-161202	P-328-161011-1439-jcr	37.94745111° N	78.95753574° W	12.0	17.2
GWNF-P327-161202	P-327-161011-1326-jcr	37.94871961° N	78.95675372° W	7.4	9.2
GWNF-P326-161202	P-326-161011-1116-jcr	37.94951126° N	78.95634975° W	8.6	15.5
GWNF-P325-161202	P-325-161011-0904-jcr	37.95016378° N	78.95593251° W	7.6	9.0
GWNF-P324-161202	P-324-161011-0850-jsw	37.95117673° N	78.95538475° W	10.1	13.6
GWNF-P323-161202	P-323-161011-0937-jsw	37.95189426° N	78.95488928° W	9.9	21.7
GWNF-R003-161202	R-003-160509-1030-mpc	37.95198079° N	78.95444245° W	8.9	16.1
GWNF-R001-161202	R-001-160509-1000-mpc	37.95241051° N	78.95450872° W	9.8	15.2
GWNF-R002-161202	R-002-160509-1015-mpc	37.95248749° N	78.95429967° W	6.4	9.3
GWNF-P322-161202	P-322-161011-0933-jsw	37.95298478° N	78.95430713° W	6.7	9.3
GWNF-P321-161202	P-321-161011-0926-jsw	37.95397658° N	78.95357976° W	10.4	12.7
GWNF-R006-161202	R-006-160509-1440-mpc	37.95448908° N	78.95337252° W	9.9	14.3
GWNF-P319-161202	P-319-161011-0929-mel	37.95579248° N	78.95322403° W	8.9	10.5

Pit ID	Soil Survey Pit ID	Lat	Long	Depth to Weathered Rock (ft)	Depth to Rock (ft)
GWNF-P318-161202	P-318-161011-1210-mel	37.95653485° N	78.95271941° W	7.3	9.7
GWNF-R005-161202	R-005-160509-1325-mpc	37.95732480° N	78.95260235° W	12.9	14.9
GWNF-R004-161202	R-004-160509-0115-mpc	37.95786916° N	78.95252239° W	10.7	14.2
GWNF-P316-161202	P-316-161011-1300-mel	37.95843763° N	78.95303423° W	10.0	12.7
GWNF-P315-161202	P-315-161011-1430-mel	37.95913432° N	78.95344385° W	9.4	12.4

Note: 1) Order 1 Soil Survey Amended Report, Atlantic Coast Pipeline, Monongahela National Forest, WV and George Washington National Forest, VA, August 1, 2016, Amended December 16, 2016, prepared by RETTEW Associates, Inc. and Geosyntec Consultants.

5.0 LIMITATIONS

This study was conducted by qualified geologists with over 36 years of collective experience in the collection, processing, and interpretation of geophysical data, including registered professional geologists. All geophysical data collection and processing are interpretive. Confirmation of these geophysical results would require invasive sampling.

6.0 REFERENCES

Fookes, P.G., Editor, 1997. Geological Society Professional Handbooks, Tropical Residual Soils, A Geological Society Engineering Group Working Party Revised Report, London.

Griffiths, D.H. and R.F. King, 1988. Applied Geophysics for Geologists & Engineers: The Elements of Geophysical Prospecting, Pergamon Press, 230 pp.

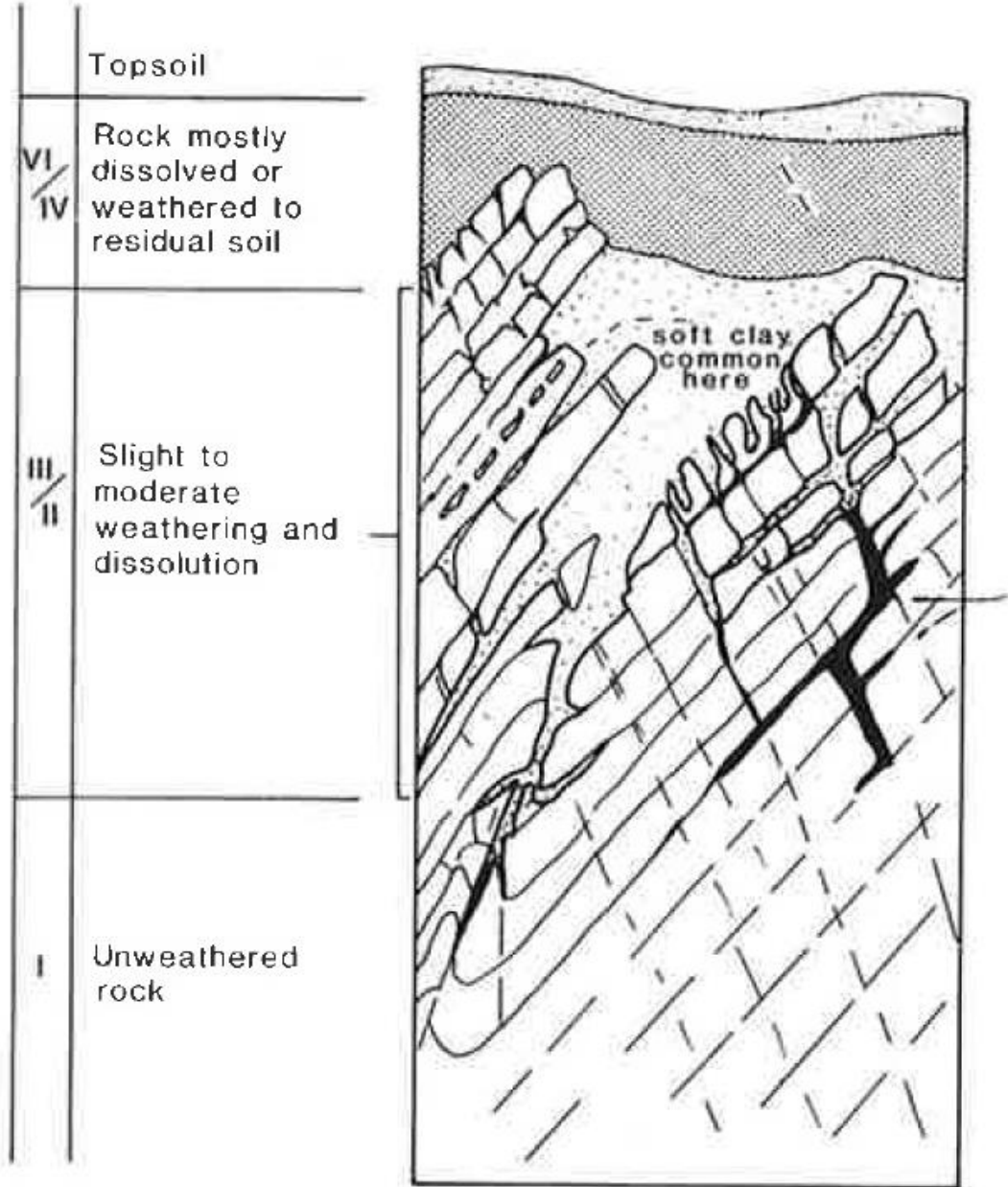
Reddy, D.V., 2010. Engineering Geology, Vikas Publishing House Pvt Ltd, New Delhi, 683 pp.

RETTEW Associates, Inc. and Geosyntec Consultants, 2016. Order 1 Soil Survey Amended Report, Atlantic Coast Pipeline, Monongahela National Forest, WV and George Washington National Forest, VA, August 1, 2016, Amended December 16, 2016.

Bourbié, T, Olivie Coussy, and Bernie Zinszner, 1987. Acoustics of Porous Media, Gulf Publishing Company, 334 pp.

7.0 FIGURES

Idealized cross-section of differential weathering



Draper Aden Associates

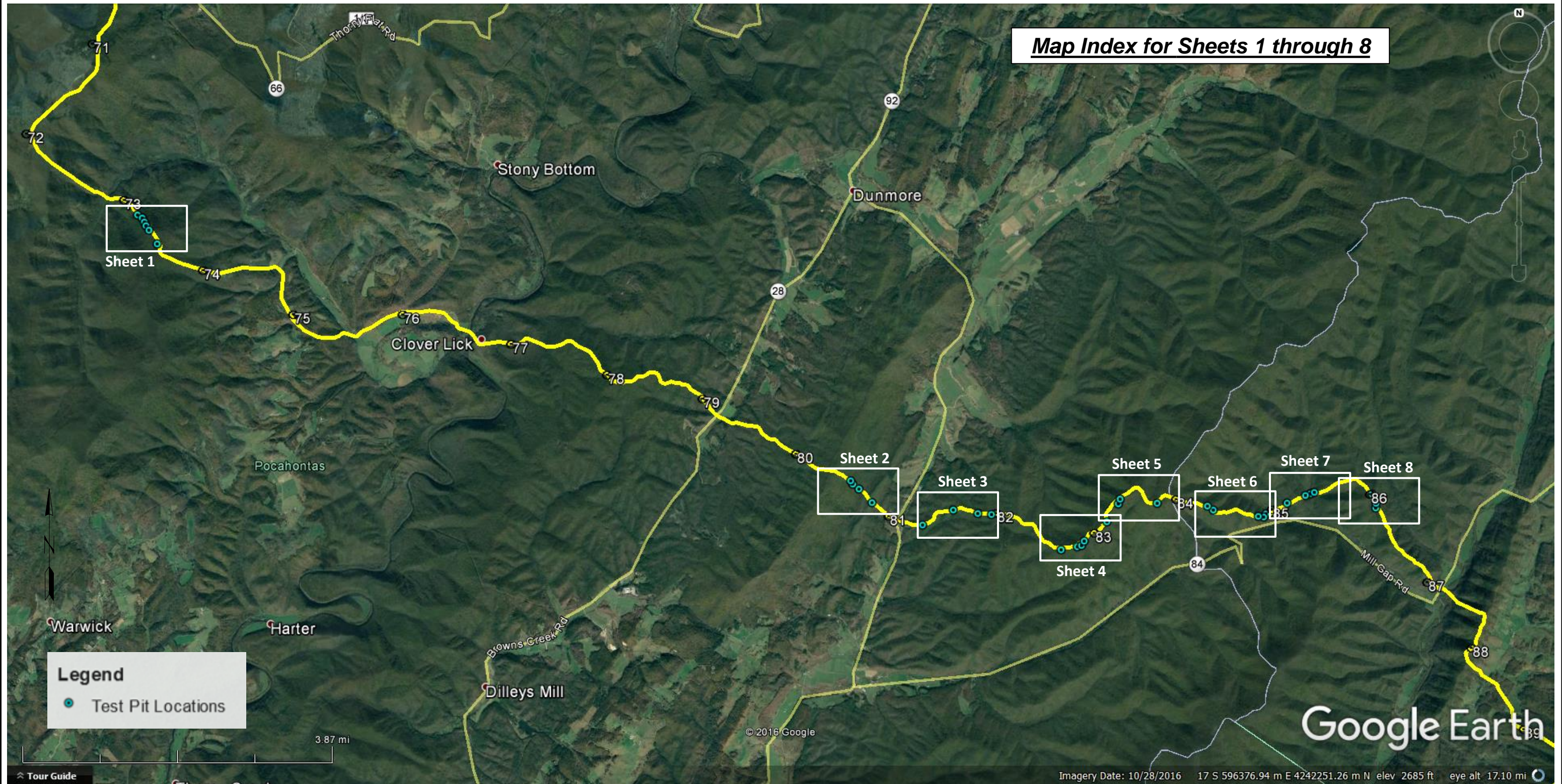
Engineering • Surveying • Environmental Services

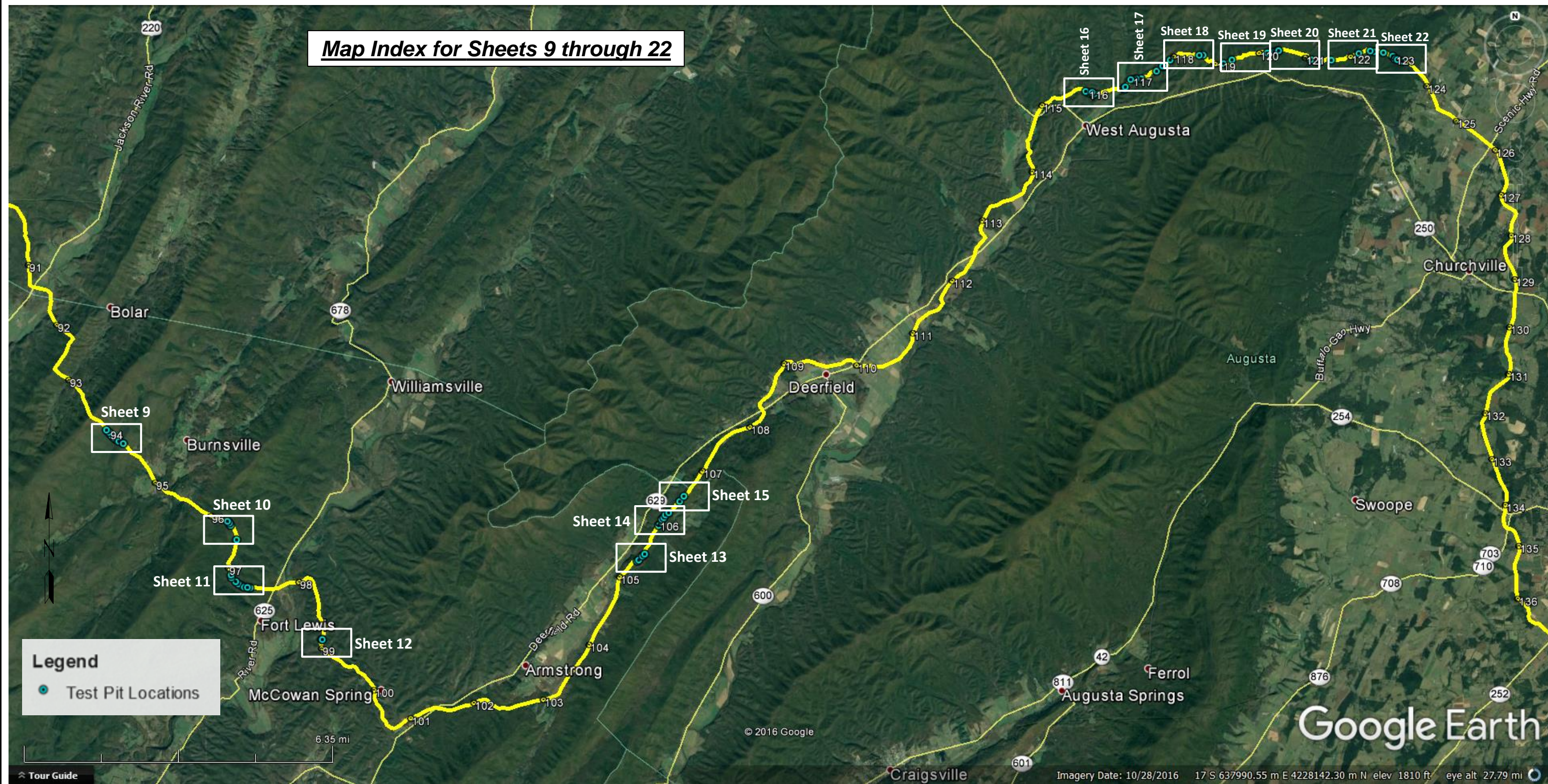
2206 South Main Street
Blacksburg, VA 24060
540-552-0444 Fax: 540-552-0291

Richmond, VA
Charlottesville, VA
Hampton Roads, VA

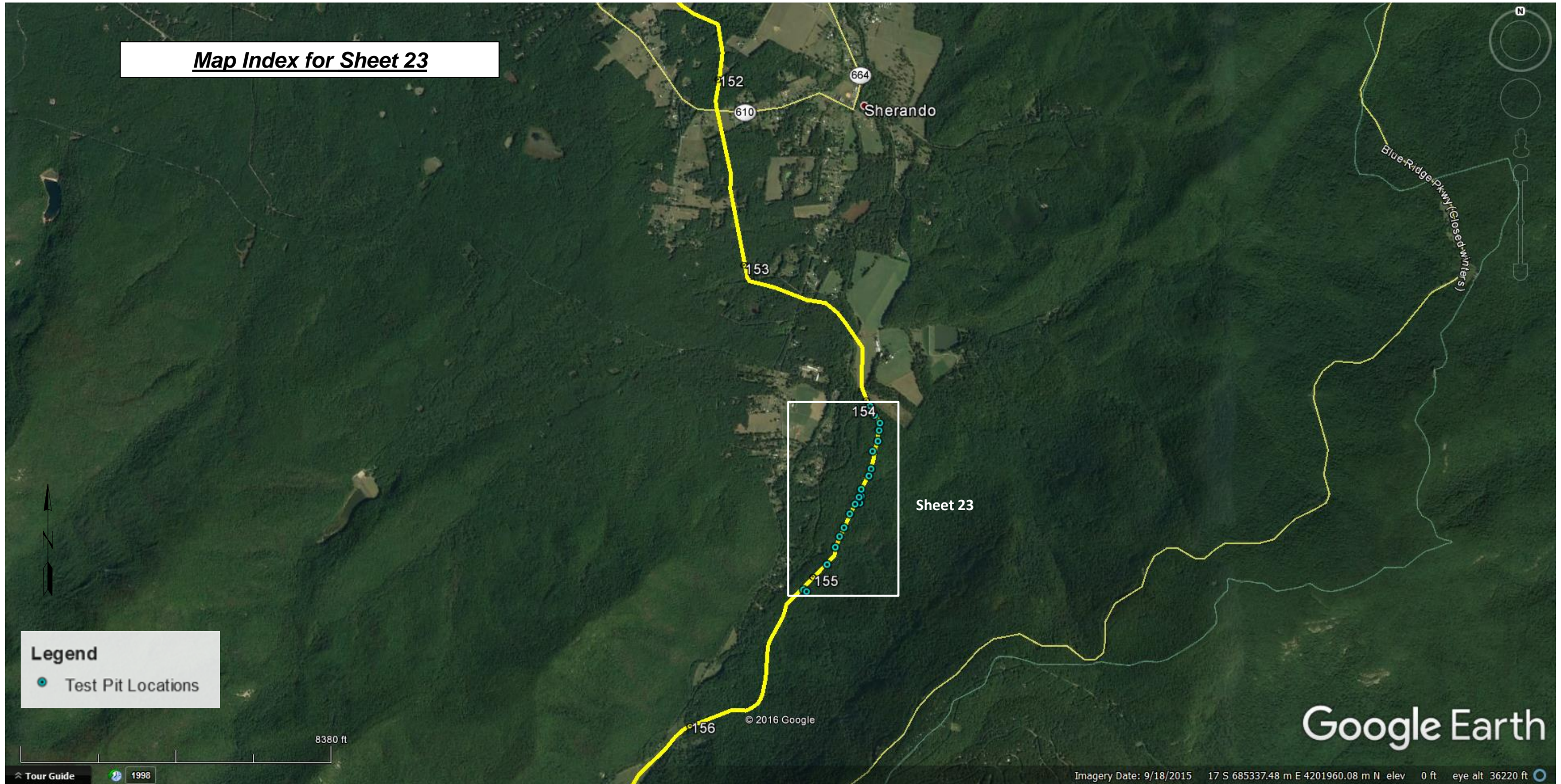
Seismic Refraction Study for the
Atlantic Coast Pipeline
George Washington National Forest and
Monongahela National Forest
DAA Project Number: 16010129-010203

FIGURE
1





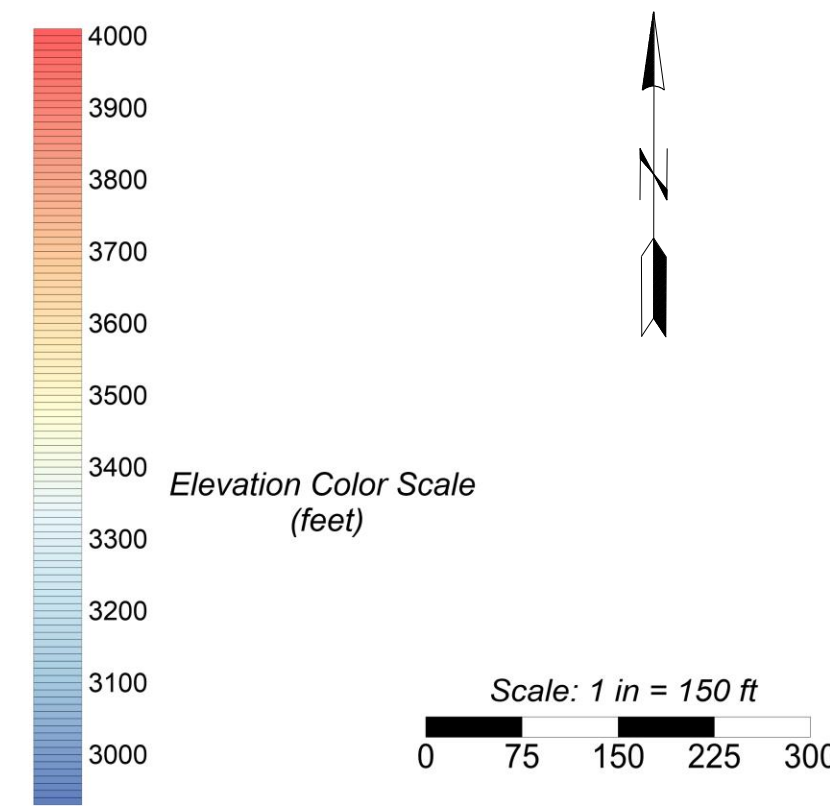
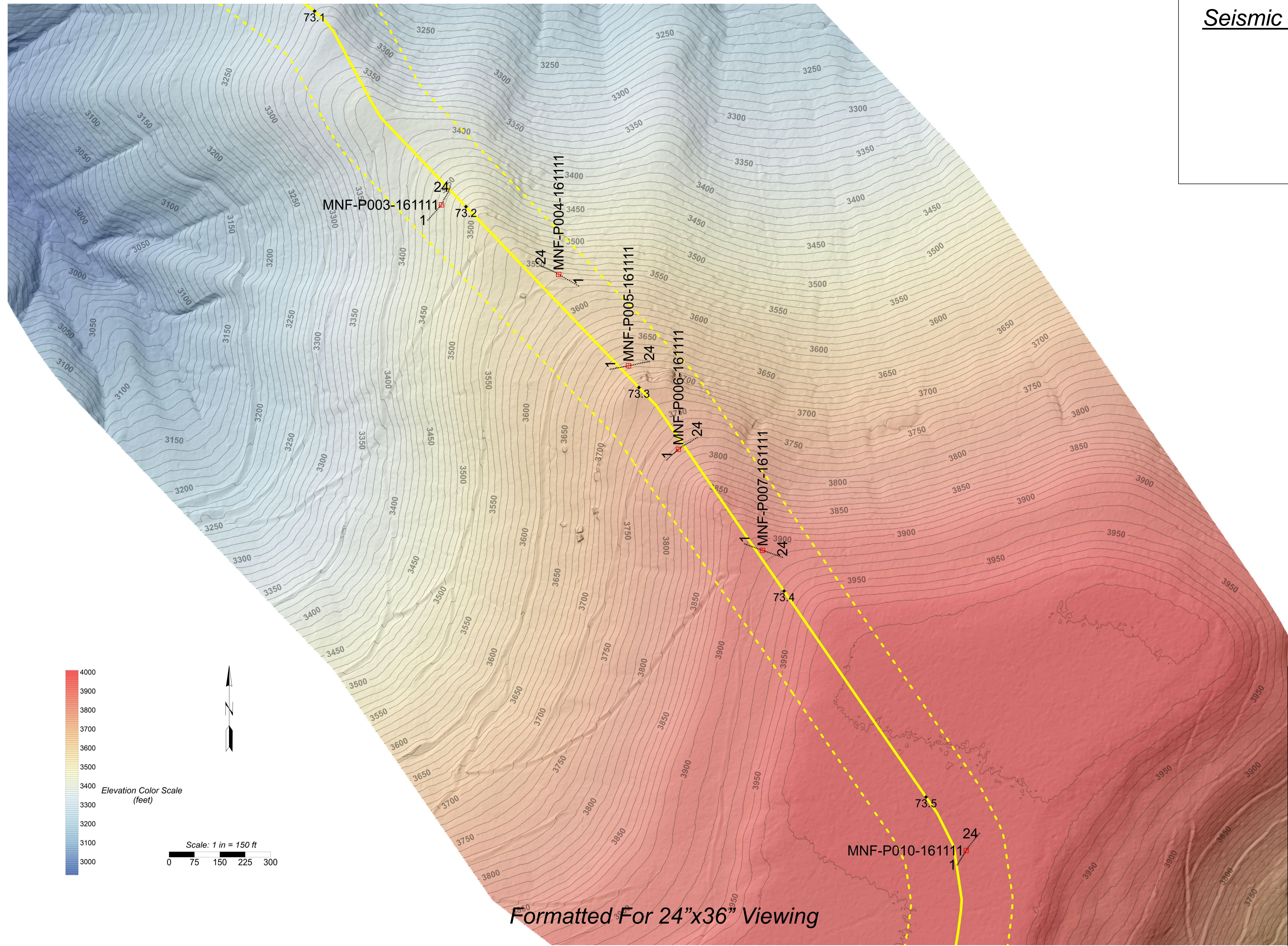
Map Index for Sheet 23



Map Sheet 1
Seismic Refraction Line Locations

Test Pits:

- MNF-P003-161111
- MNF-P004-161111
- MNF-P005-161111
- MNF-P006-161111
- MNF-P007-161111
- MNF-P010-161111



Formatted For 24"x36" Viewing

